

Set Theory-Based Safety Supervisory Control for Wind Turbines to Ensure Adequate Frequency Response

Yichen Zhang, *Student Member, IEEE*, M. Ehsan Raoufat, *Student Member, IEEE*, Kevin Tomsovic, *Fellow, IEEE*, and Seddik M. Djouadi, *Member, IEEE*

Abstract—Inadequate frequency response can arise due to a high penetration of wind turbine generators (WTGs) and requires a frequency support function to be integrated in the WTG. The appropriate design for these controllers to ensure adequate response has not been investigated thoroughly. In this paper, a safety supervisory control (SSC) is proposed to synthesize the supportive modes in WTGs to guarantee performance. The concept, region of safety (ROS), is stated for safe switching synthesis. An optimization formula is proposed to calculate the largest ROS. By assuming a polynomial structure, the problem can be solved by a sum of squares program. A feasible result will generate a polynomial, the zero sublevel set of which represents the ROS and is employed as the safety supervisor. A decentralized communication architecture is proposed for small-scale systems. Moreover, a scheduling loop is suggested so that the supervisor updates its boundary with respect to the renewable penetration level to be robust with respect to variations in system inertia. The proposed controller is first verified on a single-machine three-phase nonlinear microgrid, and then implemented on the IEEE 39-bus system. Both results indicate that the proposed framework and control configuration can guarantee adequate response without excessive conservativeness.

Index Terms—Frequency response, wind turbine generator, synthetic inertial response, safety verification, sum of squares programming, hybrid system, supervisory control.

I. INTRODUCTION

Due in part to the increasing penetration of converter-interfaced sources, such as, the wind turbine generator (WTG), total system inertia has been decreasing. The result can be inadequate system frequency response as a small power disturbance may lead to a large frequency excursion during the transient period, that is, the period of inertial and primary responses [1]–[4]. This poor transient response can trigger unnecessary over or under-frequency relay actions even though the system has adequate capacity to reach a viable steady state [5]. Thus, maintaining the system frequency within the continuous operation zone, or so-called safety¹ limits, under a certain set of disturbances has become increasingly important

This work was supported in part by the National Science Foundation under the Grant ECCS-1711432, and in part by the Engineering Research Center Program of the National Science Foundation and the Department of Energy under NSF Award Number EEC-1041877.

The authors are with the Min H. Kao Department of Electrical Engineering and Computer Science, The University of Tennessee, Knoxville, TN 37996 USA (e-mail: yzhan124@utk.edu, mraoufat@utk.edu, tomsovic@utk.edu, mdjouadi@utk.edu).

¹The term *safety* is adopted from the control literature and in this context means a well-defined and allowable operating region. A safe response means the trajectories of all concerned states stays within the defined safe limits.

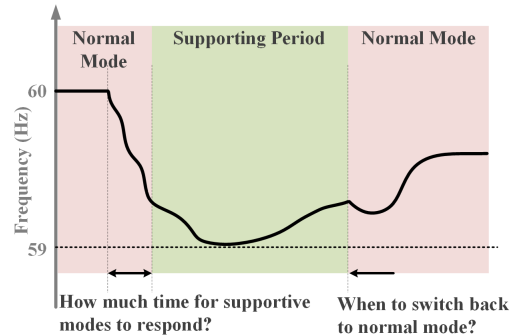


Fig. 1. Challenges of synthesizing supportive modes in CIS as the switching instants between modes to achieve an adequate frequency response are still unclear.

[5]–[7] and necessary to real-world power system operations to avoid unnecessary loss of generation and load [8].

Numerous frequency supportive functions for the WTG have been studied. These functions are supplementary to the active power control loop [9] or the phase-lock loop [10] of converter controllers. Utilizing these functions to achieve adequate frequency response, i.e., bounded within the defined safety limits for a given set of contingency events, are challenging. The first challenge is the presence of deadbands in the supportive functions. The deadbands ensure that WTGs do not respond to small frequency fluctuations in the grid so as to extract maximum power from wind [11]. Since the power extraction is the primary tasks for WTGs, the deadbands in the supplementary loops are large compared to the traditional deadbands in governors. The WTGs integrated with supportive functions become hybrid dynamical systems, where the switching between modes to achieve an adequate response are not well-understood (as illustrated in Fig. 1 [7]). In addition, a fixed deadband may not be able to handle a high penetration condition as the commitment of synchronous generators could change dramatically over time due to the stochastic characteristics of renewable sources. The second challenge for the existing controllers in WTGs is a lack of situational awareness capability as only terminal measurements are used.

A few studies on the strategies for adequate frequency response have been conducted. Ref. [5] proposed to use energy storage systems to avoid unnecessary under-frequency load shedding (UFLS). A composite model of system frequency

response (SFR) and energy storage systems is built to evaluate the enhanced frequency response, where parameters are estimated by an extended Kalman filter (EKF). A commitment strategy for interruptible load to ensure adequate response is proposed in [6]. The frequency nadir information under different commitments of interruptible load needs to be obtained via simulation and sensitivity prediction. Evaluating grid performance under support was handled via model-based estimation and simulation-based prediction in the above mentioned works. Still, the underlying hybrid behaviors due to the thresholds are not considered. Given a disturbance, the available time remaining for resources to take actions to guarantee a bounded frequency response is estimated as a function of local inertia in [7]. This reaction time can be an appropriate metric to select an adequate response action. But again, the impact of the supportive control on this reaction time is not assessed, which must be an important factor as stronger support generally should allow longer reaction time.

This paper proposes a systematic framework for synthesizing the switching between normal operation and supportive modes to ensure adequate frequency response for a given set of contingencies. The first challenge of unknown reaction time can be resolved by estimating the largest *region of safety* (ROS), which was proposed in our previous work [12] as a new concept for hybrid system safety verification. Essentially the largest ROS (LROS) is the complementary set of the backward reachable set with respect to the unsafe set. An iterative algorithm was developed in [12] to calculate the LROS. Here, to further provide convergence proof, an optimization problem in the space of continuous functions is developed according to [13]–[15]. The LROS can be estimated via the proposed formulation, which guarantees $L-1$ norm convergence to the true LROS. If the polynomial data is equipped, the problem can be solved by sum of squares (SOS) programming. The solution is a polynomial function in terms of the system states, the zero sublevel of which is the estimated LROS. When the measured states are given to the function, the output can provide a real-time margin to the critical reaction time based on the level sets and thus, switch the mode in a timely fashion to ensure response adequacy. This functionality is referred to as the safety supervisor in this paper.

Another challenge for grid performance is managed similar to [5]. A composite model of SFR and WTG is used to compute the safety supervisor. When deployed online in WTGs, the composite model serves as a state observer to provide situational awareness. The state observer and safety supervisor compose the safety supervisory control (SSC). The SSC constantly updates the boundary with respect to different renewable penetration levels and commitments of synchronous generators across stochastic renewable outputs.

The rest of the paper is organized as follows. In Section II, the optimization problem for solving the safety supervisor as well as its geometric interpretation is introduced. In Section III, the configuration of the SSC is introduced and implemented on the IEEE 39-bus system, where the dynamic performance is illustrated. Conclusions are given in Section IV.

II. SWITCHING SYNTHESIS AND SUPERVISORY CONTROL DESIGN VIA REGION OF SAFETY

A. Mathematical Framework

Consider the linearized frequency response model

$$\Delta \dot{x}_s = A_s \Delta x_s + B_s k_{\text{scal}} \Delta P_g - B_s \Delta P_d \quad (1)$$

where

$$A_s = \begin{bmatrix} 0 & 0.5/H & 0 \\ 0 & -1/\tau_T & 1/\tau_T \\ -1/(R\tau_G) & 0 & 1/\tau_G \end{bmatrix}, B_s = \begin{bmatrix} 0.5/H \\ 0 \\ 0 \end{bmatrix}$$

$$\Delta x_s = [\Delta \omega, \Delta P_m, \Delta P_v]^T$$

where ΔP_d denotes the power imbalance due to a disturbance and ΔP_g denotes the output from the WTG associated with the grid supportive controller. The generator speed, mechanical power, valve position and governor droop are denoted by ω , P_m , P_v and R , respectively. The terms H , τ_T and τ_G denote inertia constant, turbine and governor time constant, respectively. The term k_{scal} denotes a change of base if necessary. In this paper, the supportive function is limited to inertia emulation (IE) for simplicity. Let the input-output relation from the rate of change of frequency (RoCoF) signal $\dot{\omega}$ to the active power variation of the WTG ΔP_g be governed by the linear state-space model

$$\begin{aligned} \Delta \dot{x}_w &= A_w \Delta x_w + B_w s(k) k_{\text{ie}} \Delta \dot{\omega} \\ \Delta P_g &= C_w \Delta x_w + D_w s(k) k_{\text{ie}} \Delta \dot{\omega} \end{aligned} \quad (2)$$

where $s(k)$ is the unit step function to describe the switching behaviors and x_w denotes the relevant states of the WTG. The term k_{ie} is the IE gain. Let the hybrid closed-loop system of (1) and (2) be expressed in the following compact form

$$\dot{x} = f_{t_s}(x, d) \quad (3)$$

where $x = [\Delta x_s, \Delta x_w]^T$ and $d = \Delta P_d$.

The computation will be limited within a domain of interest $X \subset \mathbb{R}^n$, which can be associated with physical system limits. Assume a power imbalance occurs at time t_0 . The objective of the SSC is to activate the WTG supportive controller at time $k = t_0 + t_s$ so that the frequency response is adequate, i.e., $\omega \in X_S = \{x | \omega_{\text{lim}}^- \leq \omega \leq \omega_{\text{lim}}^+\} \cap X$. The set X_S is usually denoted as *safe set*, and its complementary set is called the *unsafe set* $X_U = \{x | \omega > \omega_{\text{lim}}^+ \text{ or } \omega < \omega_{\text{lim}}^-\} \cap X$. The frequency safety limits are usually defined for a set of contingencies, i.e., $d \in D = \{\delta | \delta_{\text{lim}}^- \leq \delta \leq \delta_{\text{lim}}^+\}$. Let X_I be the initial set, $\phi(t|x_0, d)$ be the trajectory initialized in $x_0 \in X_I$. Two concepts are defined as follows [12].

Definition 1 (Safety): Given (3), X , X_I , X_U and D , the *safety property* holds if there exists no time instant $T \geq 0$ and no piecewise constant bounded disturbance $d : [0, T] \rightarrow D$ such that $\phi(t|x_0, d) \cap X_U \neq \emptyset$ for any $t \in [0, T]$ and any $x_0 \in X_I$.

Definition 2 (Region of Safety): A set that only initializes trajectories with the property in Definition 1 is called a *region of safety*.

Having defined these concepts, the switching synthesis principle via ROS can be interpreted as given in Fig. 2. Consider two extreme scenarios of the hybrid system in (3) when

$t_s = \infty$ and $t_s = 0$, respectively. The first one presents the vector field under the maximum power point tracking (MPPT) mode $f_\infty(x, d)$ and the latter one denotes the SFR under the inertia emulation mode without deadband $f_0(x, d)$. Assume the ROSs under the different vector fields are calculated for $d \in D$ and shown as the green areas in Fig. 2. Due to the inertia emulation support, the ROS under its vector field is larger. When the system undergoes a contingency, a switching that guarantees adequate response can be found as long as the trajectory is inside the ROS of $f_0(x, d)$. Since the states cannot jump, the trajectory after switching will be initialized within the ROS and according to Definition 2 it is safe. Since the ROS is obtained in the form of a zero sublevel set of a continuous function of system states $B_0(x) \leq 0$, the remaining margin to the critical switching instant can be easily found by pushing the value towards zero. It is worth distinguishing the ROS from the region of attraction (ROA) as a safe trajectory may cross the boundary of the ROS. The general principle of safe switching synthesis is subscribed by the following proposition [12].

Proposition 3: In a hybrid system with several modes, let the ROS and trajectory of mode i be denoted by $S_i = \{x | B_i(x) \leq 0\}$ and $\phi_i(t)$, respectively. A safe switching from mode i to mode j at t_s is guaranteed if $\phi_i(t_s) \in S_j$, that is, $B_j(\phi_i(t_s)) \leq 0$.

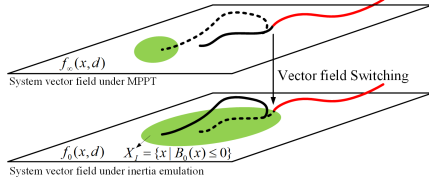


Fig. 2. Switching principle under guidance of ROS for safe trajectory. The boxes are the safety limits. The green areas are the ROS of corresponding vector fields. The solid black lines are safe trajectories while the solid red ones are unsafe. The dash lines are trajectory projected onto the other vector field.

It is clear that the key to appropriately supervising the mode switching is to estimate as close as possible the true LROS X_I^* . The LROS can be explained in the reachability sense. Consider a computation domain of interest X consisting of the safe set X_S and unsafe set X_U as illustrated in Fig. 3. The true and estimated invariant backward reachable set (BRS) of X_U is denoted as X_B^* and \bar{X}_B , respectively. Every trajectory starting in X_B^* will reach the unsafe set. Thus, the LROS is the relative complement of X_B^* with respect to X_S , i.e., $X_I^* = X_S \setminus X_B^*$. The BRS can be estimated by either solving the Hamilton-Jacobi partial differential equation (PDE) [16] [17] or operating sets in the form of ellipsoids [18] or zonotopes [19]–[21]. The Hamilton-Jacobi PDE approach has good convergence characteristics, but suffers from a heavy computational burden and does not scale to higher order systems. The set operation methods can be applied to more general systems due to the choice of special representations of sets, but this leads to over-approximation.

A recent novel approach proposed in [13]–[15] uses occupation measures to formulate the BRS computation as an infinite-dimensional linear program. Its dual problem is formulated on

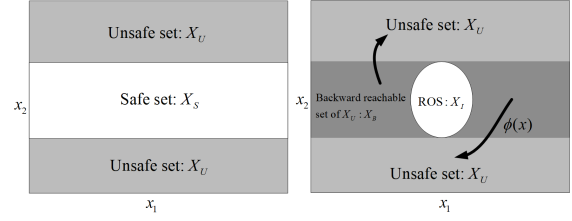


Fig. 3. ROS interpretation in reachability sense.

the space of nonnegative continuous functions. Based on [14], we propose the optimization problem (4) under the vector field $t_s = 0$

$$\inf_{B(x), \Omega(x)} \int_X \Omega(x) d\lambda(x) \quad (4a)$$

$$\text{s.t.} \quad B(x) > 0 \quad \forall x \in X_U \quad (4b)$$

$$\frac{\partial B}{\partial x} f_0(x, d) \leq 0 \quad \forall (x, d) \in X \times D \quad (4c)$$

$$\Omega(x) \geq B(x) + 1 \quad \forall x \in X \quad (4d)$$

$$\Omega(x) \geq 0 \quad \forall x \in X \quad (4e)$$

where the computation domain X , unsafe set X_U and disturbance set D are given. The infimum is over $B \in C^1(X)$ and $\Omega \in C(X)$. λ denotes the Lebesgue measure. If the problem is feasible, the safety $f_0(x, d)$ with $d \in D$ is preserved and the zero level set of $\Omega(x) - 1$ converges below to X_I^* .

A strict mathematical proof is out of the scope of this paper. Instead, a geometric interpretation is given. In essence, the problem in (4) tries to estimate the BRS in Fig. 3 without knowing the initial set X_0 . Let any trajectory eventually ending up in the set X_U at certain time T be denoted as $\phi(T|x_0)$. Based on the conditions of $B(\phi(T|x_0)) > 0$ in (4b) and the passivity in (4c), one can easily show $B(x_0) > 0$. Thus, (4b) and (4c) ensure that $B(x) > 0$ for any $x \in X_B^*$ illustrated as a one dimensional case in Fig. 4. The conservatism lies in the fact that $B(x) > 0$ for some $x \in X_I^*$, which overestimates the BRS (i.e., $X_B^* \subset \bar{X}_B$) and in turn underestimates the ROS (i.e., $X_I^* \supset \bar{X}_I$). Fortunately, this conservatism can be reduced by introducing a positive slack function $\Omega(x)$ that is point-wise above the function $B(x) + 1$ over the computation domain X . Assume the complement set of X_I^* is represented by the indicator function $\delta_{X \setminus X_I^*}(x)$, i.e., a function is equal to one on $X \setminus X_I^*$ and 0 elsewhere. The key idea of the problem in (4) is that by minimizing the area of function $\Omega(x)$ over the computation domain X , the function $B(x) + 1$ will be forced to approach $\delta_{X \setminus X_I^*}(x)$ from above as shown in Fig. 4. Thus, the zero sublevel set of $\Omega(x) - 1$ is an inner approximation of X_I^* . Essentially, the problem in (4) is trying to approximate an indicator function using a polynomial. The conservatism of the estimate vanishes with increasing order of the polynomial.

Obviously the problem in (4) attains its optimum when $\delta_{X \setminus X_I^*}(x) = B(x) + 1 = \Omega(x)$. If all functions are confined to be polynomials and all sets are basic closed semi-algebraic sets (hence defined by finitely many polynomial inequalities and equality constraints) [22], then the recent SOS decomposition techniques [23] can reformulate problem (4) into a SOS

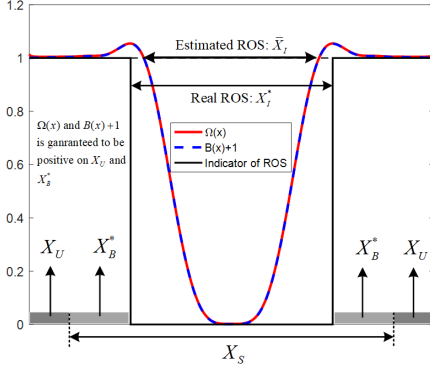


Fig. 4. Geometry interpretation of proposed optimization problem for estimating the ROS.

program, which can be further converted into a semi-definite program (SDP). This procedure has been implemented in several toolboxes such as Yalmip [24]. The SOS program to solve problem (4) is given as follows.

Let $X = \{x \in \mathbb{R}^n | g_X(x) \geq 0\}$, $X_U = \{x \in \mathbb{R}^n | g_U(x) \geq 0\}$, and $D = \{d \in \mathbb{R}^m | g_D(d) \geq 0\}$, which are represented by the zero superlevel set of the polynomials $g_X(x)$, $g_U(x)$, and $g_D(d)$, respectively, and some small positive number ϵ be given. Functions $B(x)$ and $\Omega(x)$ are polynomials with fixed degree. Multipliers $\sigma_i(x)$ for $i = 1, \dots, 6$ are SOS polynomials with fixed degree. Then the ROS can be obtained by solving the following SOS program

$$\inf_{B(x), \Omega(x)} \omega^l \quad (5a)$$

$$B(x) - \epsilon - \sigma_1(x)g_U(x) \in \Sigma^2[x] \quad (5b)$$

$$-\frac{\partial B}{\partial x}(x)f_0(x, d) - \sigma_2(x, d)g_D(d) \quad (5c)$$

$$-\sigma_3(x, d)g_X(x) \in \Sigma^2[x]$$

$$\Omega(x) - B(x) - 1 - \sigma_4(x)g_X(x) \in \Sigma^2[x] \quad (5d)$$

$$\Omega(x) - \sigma_5(x)g_X(x) \in \Sigma^2[x] \quad (5e)$$

where l is the vector of the moments of the Lebesgue measure over X indexed in the same basis in which the polynomial $\Omega(x)$ with coefficients ω is expressed. For example, for a two-dimensional case, if $\Omega(x) = c_1x_1^2 + c_2x_1x_2 + c_3x_2^2$, then $\omega = [c_1, c_2, c_3]$ and $l = \int_X [x_1^2, x_1x_2, x_2^2] dx_1 dx_2$.

B. Illustrative Example: a Diesel/Wind fed Microgrid

To illustrate the SSC design using the proposed framework, a lumped diesel/wind fed microgrid in [25] is investigated. Assume that the parameters of the frequency response model of the diesel generator in the form of (1) have been estimated. The WTG model used in the SSC design is a first-order linear system obtained using the selective modal analysis based model reduction [26] and proved to be precise in capturing the input-output relation from the supplementary signal to the

active power variation [12]. The rotor speed of WTG is the state, i.e., $\Delta x_w = \Delta \omega_r$. The parameters are given as follows

$$H = 2, R^{-1} = 30, \tau_G = 0.1, \tau_T = 0.5$$

$$A_w = -0.3914, B_w = -0.3121, C_w = 1.37, D_w = 1$$

$$k_{scal} = 0.15, k_{ie} = 0.2, \Delta P_d \in D = \{d | 0 \leq d \leq 0.32\}$$

and the states of the overall frequency response model including synthetic inertial response are $x = [\Delta \omega, \Delta P_m, \Delta P_v, \Delta \omega_r]$. The safety limit is set as $\omega_{lim}^- = 58.5$ Hz, intentionally leaving no extra margin. With all the given conditions, the problem in (5) is formulated in Yalmip [27] and solved by Mosek [28]. The ROS is represented by the zero sublevel set of $B(x)$ and its projection on the phase plane of frequency and mechanical power is shown in Fig. 5. The blue region is the ROS obtained by massive simulations and can be considered as the "true" region. As shown by minimizing the area under the slack function $\Omega(x)$, the zero level set of $B(x)$ is expanded by $\Omega(x) - 1$ as much as possible to the true LROS under a fixed highest degree.

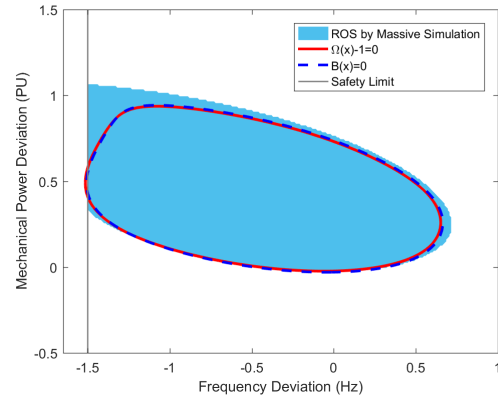


Fig. 5. Comparison of ROS (projected onto $\Delta \omega - \Delta P_m$ plane) between the subzero level set of $B(x)$ (blue dash) and exhaustive simulations (blue).

Once $B(x)$ is obtained, it can be deployed online in the configuration shown in Fig. 6. The speeds of diesel and wind turbine generators are measurable. The estimated frequency response model used in ROS computation is now employed as the state observer for ΔP_m and ΔP_v . The SSC integrated into WTGs not only enables the situational awareness capability, but also provides a real-time margin towards safe switching.

To show in a simulation, the full-order nonlinear model of a synchronous generator is used but scaled down to microgrid rating. A type-4 wind turbine with an averaged converter model is used. Detailed description of model used in simulation can be found in [25]. The system under the worse-case disturbance is simulated. The frequency response and the value of safety supervisor are shown in Fig. 7. The IE is activated when the supervisor's value crosses zero. As seen, the nadir of the frequency response with activated SSC is exactly at the safety limit, indicating the estimated LROS is not conservative.

of base as $k_{\text{scal}} = S_{\text{wt}}/S_{\text{sg}}$, one can have the overall model in the form of (3) for ROS computation.

B. Decentralized Communication for Small-scale Systems

Based on the theoretical model developed in Section III-A, a centralized communication link shown in Fig. 9 (a) is needed for the SSC. The speed of each synchronous generator (area) is measured and transmitted to the central controller to calculate the COI frequency. Then, the COI frequency is sent to state observers to estimate states $\Delta\bar{P}_m$, $\Delta\bar{P}_v$, $\Delta\bar{x}$ and $\Delta\bar{\omega}_r$. Finally, all the states are substituted into the safety supervisor to make switching decisions. This switching signal needs to be transmitted to each WTG to activate the inertia emulation. Although such a communication architecture could theoretically ensure the safe response of the COI frequency, it would likely introduce excessive delay and complexity, reduce reliability and require additional infrastructure cost.

Essentially, the WTGs only need the switching signal, which is determined by predicting overall system behavior. Since frequency is a global feature, the system awareness capability can be integrated locally in each WTG using the same state observer. Then, as long as the input is the COI frequency, the result will be the same. In order to further reduce the communication links, measuring local frequency is desired. It is known that the local frequency will deviate from the COI frequency during transient period. But for a small-scale system, such deviations should be small. Thus, it is reasonable to assume that the frequency of single machine (area) approximates the COI frequency, i.e., $\omega_i \approx \bar{\omega}$. Therefore, the centralized SSC can be replaced by a decentralized SSC as shown in Fig. 9 (b). The decentralized SSC is completely integrated into a single WTG, and only local frequency measure are needed. Still, such communication reduction is only equivalent when the system is small.

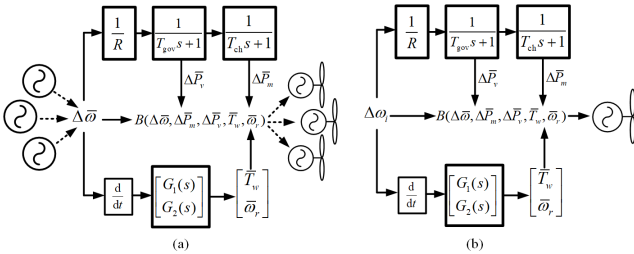


Fig. 9. Centralized and decentralized communication in SSC. The decision results will be equivalent for a small scale system.

C. Simulation to Verify Dynamic Performance

In this subsection, the modified New England IEEE 39-bus system with more than 50% wind generation is used to demonstrate the SSC. Two scenarios with varying levels of wind generation used as actuators and different inertia emulation gains are illustrated.

The modified generator data of the system is listed in Table I. All other parameters are the same as the standard model. The bold inertia constants indicate that they are

TABLE I
GENERATOR DATA OF MODIFIED NEW ENGLAND 39-BUS SYSTEM

#	Bus	Type	Output (MW)	Base (MVA)	Inertia (s)
1	30	WTG	550	$S_1 = 670$	$H_1 = 8.00$
2	31	WTG	572	$S_2 = 670$	$H_2 = 8.00$
3	32	WTG	650	$S_3 = 670$	$H_3 = 8.00$
4	33	SG	632	$S_4 = 1000$	$H_4 = \mathbf{2.86}$
5	34	WTG	508	$S_5 = 670$	$H_5 = 8.00$
6	35	WTG	650	$S_6 = 670$	$H_6 = 8.00$
7	36	SG	400	$S_7 = 1000$	$H_7 = \mathbf{2.64}$
8	37	WTG	540	$S_8 = 670$	$H_8 = 8.00$
9	38	SG	830	$S_9 = 1000$	$H_9 = \mathbf{3.45}$
10	39	SG	859	$S_{10} = 1000$	$H_{10} = \mathbf{5.00}$

visible to the grid. The synchronous generators are round rotor models equipped with 1992 IEEE type DC1A excitation system model (ESDC1A) and steam turbine-governor model (TGOV1) [34]. The Western Electricity Coordinating Council (WECC) generic type-3 WTG model with built-in controls in [33] is implemented as a user-defined model (UDM). The SSC is implemented by using dynamically linked blocks (DLBs) in C/C++, which allows for advanced control implementation [35]. The overall dynamic simulation is performed in TSAT [36].

The traditional plant pool is $\mathcal{S} = \{4, 7, 9, 10\}$. The worst-case contingency is the loss of an entire traditional plant, unit 7, which is a 400 MW generation loss. The safety limit is set to be 59 Hz. In the New England system, frequencies of individual machines are close to the COI frequency. Considering the fact that UFLS rely allows frequency to stay in the triggering zone for several cycles, it is adequate to ensure the safety of the COI frequency response. This is also for the purpose of demonstrating the precision of the proposed framework.

In the first scenario, only WTG 5 is selected as the actuator equipped with $k_{ie} = 0.2$. The power and current limits are modified to assume an over-sized design of the converters. Under the worst-case contingency, the COI frequencies of the no switching case and supervised switching one are compared in Fig. 10 (a). As seen, the supervisory control timely activates the IE function of WTG 5 based on the supervisory value (shown in Fig. 10 (b)) so that the COI frequency stays within the specified safety limit. Since the supportive gain is large, there is approximately a one second reaction time for WTG 5 to respond. Individual synchronous generator speeds are also plotted. As seen, they are close to the COI frequency. So ensuring safe COI frequency response will greatly reduce the possibility of unnecessary frequency relay actions.

In the second scenario, three WTGs are chosen to be actuators, i.e., $\mathcal{W} = \{1, 2, 5\}$, with a smaller gain of $K_{ie} = 0.03$ so that each WTG will not reach its normal design limit. The same contingency is applied. The COI frequency and frequencies of individual synchronous generators are plotted in Fig. 11 (a). Fig. 11 (b) indicates that the IE function is activated at slightly different times, from 0.4 to 0.6 s in the different WTGs. This is because the slight difference in the local frequencies. The power outputs of WTG 1, 2 and 5 are shown in Fig. 12. Each of them contributes less than 0.1 per unit deviation from their nominal operating points, while

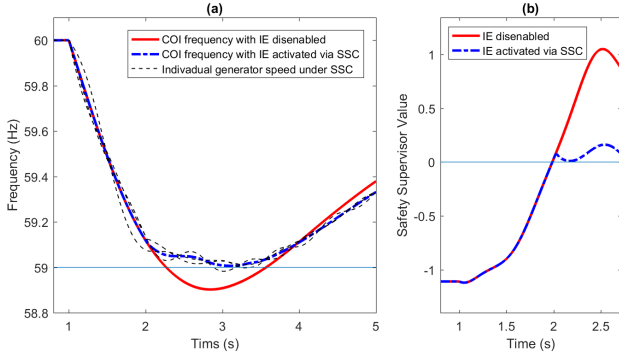


Fig. 10. Frequency response under no inertia emulation and inertia emulation activated via safety supervisory control (SSC), (a) frequency response, (b) value of safety supervisor. The reaction time is around one second in this scenario.

WTG 5 contributes more than 0.15 per unit. It is generally preferred to coordinate more actuators to reduce the required contribution from each one.

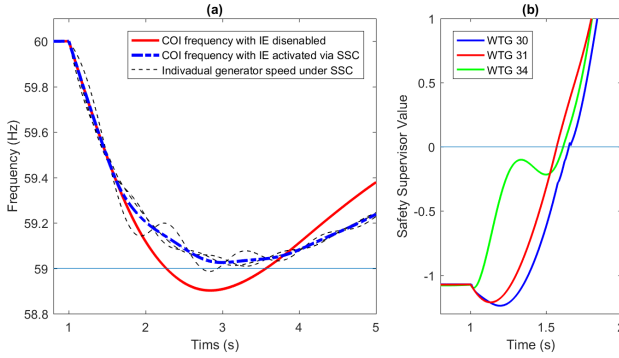


Fig. 11. Frequency response under no inertia emulation and inertia emulation activated via safety supervisory control (SSC), (a) frequency response, (b) value of safety supervisor. The reaction time is from 0.4 to 0.6 second in different WTGs in this scenario.

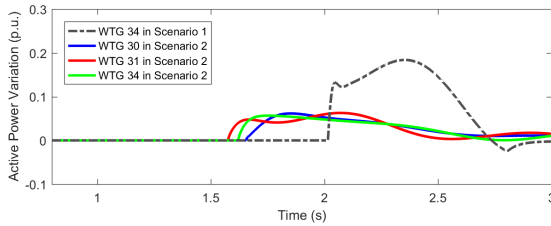


Fig. 12. Active power variation of WTGs in different scenarios.

D. Adaptive SSC against Varying Renewable Penetration

Due to the stochastic nature of renewable resources, the commitment of traditional plants can change dramatically over time, which could significantly change the system frequency response. This time-varying feature requires a SSC to be adaptive to the system operating condition. This adaptivity can be implemented by adding a scheduling loop overseeing the triggering loop as shown in Fig. 13. The triggering loop will

receive local measurements and make a decision if the condition is fulfilled. On the other hand, the scheduling loop will receive global scheduling signals, such as, unit commitment and WTG outputs, and then recalculate settings for the safety supervisor. The scheduling loop can be executed at certain intervals. When choosing actuators, those with larger capacity will be selected first. If the SOS program is not feasible, then more WTGs are needed.

It is necessary to update the supervisor periodically due to the intermittent and stochastic nature of renewables. Based on the setting of Scenario 1, assume in certain parts of the Eastern Interconnections the wind power increases dramatically over a time window and considerable numbers of synchronous generators are shut down. This change can be equivalently represented by decreasing the inertia constant of SG 10 from 10 seconds to 1 second. Using the safety setting in Section III-C, the ROSs under different operating conditions are computed and plotted in Fig. 14 (a). The same disturbance is applied under the condition when $H_{10} = 1$ second and the trajectory is plotted in Fig. 14 (a) as well. The adequate reaction time should be around 0.2 s based on the up-to-date supervisor (blue). If not updated in time, the inertia emulation may be not able to activated timely as shown in Fig. 14 (b).

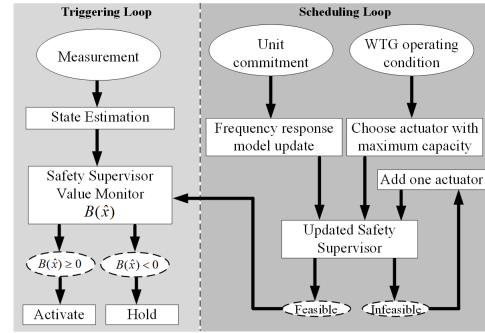


Fig. 13. Two-loop SSC with adaptivity and robust to the change of system operating point.

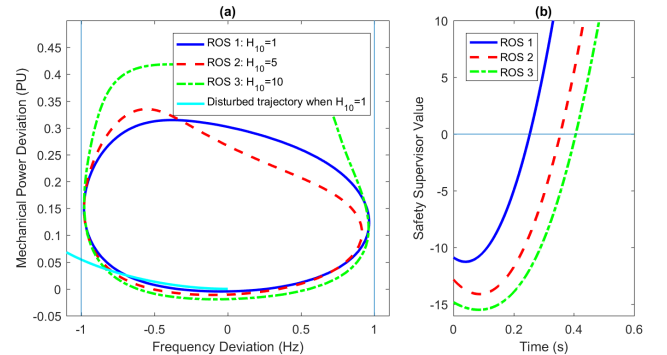


Fig. 14. (a) ROSs under different operating conditions. (b) Values of different supervisors with respect to the disturbed trajectory when $H_{10} = 1$ s.

IV. SUMMARY

This paper first interprets the mode synthesis principle for safe response and the concept of ROS. Then, a mathematical

optimization problem in the functional space is proposed to estimate the LROS. The optimization problem is explained from a geometric point of view, and then converted into a SOS program by using polynomial functions and semi-algebraic sets. A feasible result of the SOS program will generate a barrier certificate. The superlevel set of the barrier certificate over-approximates the backward reachable set of the unsafe set and the sublevel set of it under-approximates the ROS. This barrier certificate is employed as the safety supervisor for hybrid supportive mode synthesis of WTGs. The proposed controller is verified on a single-machine three-phase nonlinear microgrid model in Simulink. For multi-machine systems, a decentralized SSC is designed for small-scale systems and demonstrated on the IEEE 39-bus system with high renewables modeled in DSATools. Both results indicate that the proposed framework and control configuration will ensure adequate response with relatively little conservativeness. Finally, a scheduling loop is proposed so that the supervisor updates its boundary with respect to the renewable penetration level so as to be robust against variations in system inertia. The shape change of ROSs with respect to renewable penetration level is demonstrated. Future work will focus on reducing computational complexity.

REFERENCES

- [1] N. W. Miller, M. Shao, and S. Venkataraman, "California ISO (CAISO) frequency response study," General Electric International, Inc., Schenectady, NY, USA, Tech. Rep., Nov. 2011.
- [2] N. Miller, M. Shao, S. Pajic, and R. D'Aquila, "Eastern frequency response study," Nat. Renew. Energy Lab., Golden, CO., USA, Tech. Rep. NREL/SR-5500-58077, May 2013.
- [3] P. Mackin, R. Daschmans, B. Williams, B. Haney, R. Hunt, and J. Ellis, "Dynamic simulations studies of the frequency response of the three u.s. interconnections with increased wind generation," Lawrence Berkeley Nat. Lab., Berkeley, CA, USA, Tech. Rep. LBNL-4146E, Dec. 2010.
- [4] V. Gevorgian, Y. Zhang, and E. Ela, "Investigating the impacts of wind generation participation in interconnection frequency response," *IEEE Trans. Sustain. Energy*, vol. 6, no. 3, pp. 1–9, 2014.
- [5] S. Pulendran and J. E. Tate, "Energy storage system control for prevention of transient under-frequency load shedding," *IEEE Trans. Smart Grid*, vol. 8, no. 2, pp. 927–936, 2017.
- [6] R. Bhana and T. J. Overbye, "The commitment of interruptible load to ensure adequate system primary frequency response," *IEEE Trans. Power Syst.*, vol. 31, no. 3, pp. 2055–2063, 2016.
- [7] F. M. Uriarte, C. Smith, S. VanBroekhoven, and R. E. Hebner, "Micro-grid ramp rates and the inertial stability margin," *IEEE Trans. Power Syst.*, vol. 30, no. 6, pp. 3209–3216, 2015.
- [8] J. Brisebois and N. Aubut, "Wind farm inertia emulation to fulfill hydro-quebec's specific need," in *Proc. 2011 IEEE Power and Energy Soc. General Meeting*, 2011, pp. 1–7.
- [9] Y. Li, Z. Xu, and K. P. Wong, "Advanced control strategies of PMSG-based wind turbines for system inertia support," *IEEE Trans. Power Syst.*, vol. 32, no. 4, pp. 3027–3037, 2017.
- [10] W. He, X. Yuan, and J. Hu, "Inertia provision and estimation of PLL-based dfig wind turbines," *IEEE Trans. Power Syst.*, vol. 32, no. 1, pp. 510–521, 2017.
- [11] F. Wilches-Bernal, J. H. Chow, and J. J. Sanchez-Gasca, "A fundamental study of applying wind turbines for power system frequency control," *IEEE Trans. Power Syst.*, vol. 31, no. 2, pp. 1496–1505, 2016.
- [12] Y. Zhang, K. Tomsovic, S. Djouadi, and H. Pulgar-Painemal, "Hybrid controller for wind turbine generators to ensure adequate frequency response in power networks," *IEEE J. Emerg. Sel. Topics Circuits Syst.*, vol. 7, no. 3, pp. 359–370, 2017.
- [13] M. Korda, D. Henrion, and C. N. Jones, "Inner approximations of the region of attraction for polynomial dynamical systems," in *Proceedings of the 9th IFAC Symposium on Nonlinear Control Systems*, 2013, pp. 534–539.
- [14] D. Henrion and M. Korda, "Convex computation of the region of attraction of polynomial control systems," *IEEE Trans. Autom. Control*, vol. 59, no. 2, pp. 297–312, 2014.
- [15] M. Korda, D. Henrion, and C. N. Jones, "Convex computation of the maximum controlled invariant set for polynomial control systems," *SIAM Journal on Control and Optimization*, vol. 52, no. 5, pp. 2944–2969, 2014.
- [16] C. J. Tomlin, I. Mitchell, A. M. Bayen, and M. Oishi, "Computational techniques for the verification of hybrid systems," *Proc. IEEE*, vol. 91, no. 7, pp. 986–1001, 2003.
- [17] I. M. Mitchell, A. M. Bayen, and C. J. Tomlin, "A time-dependent hamilton-jacobi formulation of reachable sets for continuous dynamic games," *IEEE Trans. Autom. Control*, vol. 50, no. 7, pp. 947–957, 2005.
- [18] Y. C. Chen and A. D. Domínguez-García, "A method to study the effect of renewable resource variability on power system dynamics," *IEEE Trans. Power Syst.*, vol. 27, no. 4, pp. 1978–1989, 2012.
- [19] J. N. Maidens, S. Kaynama, I. M. Mitchell, M. M. Oishi, and G. A. Dumont, "Lagrangian methods for approximating the viability kernel in high-dimensional systems," *Automatica*, vol. 49, no. 7, pp. 2017–2029, 2013.
- [20] M. Althoff and B. H. Krogh, "Reachability analysis of nonlinear differential-algebraic systems," *IEEE Trans. Autom. Control*, vol. 59, no. 2, pp. 371–383, 2014.
- [21] M. Althoff, "Formal and compositional analysis of power systems using reachable sets," *IEEE Trans. Power Syst.*, vol. 29, no. 5, pp. 2270–2280, 2014.
- [22] D. Henrion, J. B. Lasserre, and C. Savorgnan, "Approximate volume and integration for basic semialgebraic sets," *SIAM Rev.*, vol. 51, pp. 722–743, 2009.
- [23] P. A. Parrilo, "Structured semidefinite programs and semialgebraic geometry methods in robustness and optimization," Ph.D. dissertation, Calif. Inst. Technol., Pasadena, CA, 2000.
- [24] J. Löfberg, "Pre-and post-processing sum-of-squares programs in practice," *IEEE Trans. Autom. Control*, vol. 54, no. 5, pp. 1007–1011, 2009.
- [25] Y. Zhang, A. Melin, S. Djouadi, and M. Olama, "Performance guaranteed inertia emulation for diesel-wind system feed microgrid via model reference control," in *Proc. IEEE PES Innov. Smart Grid Technol. (ISGT)*, 2017, pp. 1–5.
- [26] H. A. Pulgar-Painemal, "Wind farm model for power system stability analysis," Ph.D. dissertation, Univ. of Illinois at Urbana-Champaign, Champaign, IL, 2010.
- [27] J. Löfberg, "YALMIP: A toolbox for modeling and optimization in MATLAB," in *Proc. IEEE CCA/ISIC/CACSD Conf.*, Taipei, Taiwan, 2004. [Online]. Available: <http://users.isy.liu.se/johanl/yalmip/>
- [28] *The MOSEK optimization toolbox for MATLAB manual. Version 7.1 (Revision 28)*, MOSEK ApS, 2015. [Online]. Available: <http://docs.mosek.com/7.1/toolbox/index.html>
- [29] P. M. Anderson and M. Mirheydar, "A low-order system frequency response model," *IEEE Trans. Power Syst.*, vol. 5, no. 3, pp. 720–729, 1990.
- [30] I. A. Hiskens, "Dynamics of type-3 wind turbine generator models," *IEEE Trans. Power Syst.*, vol. 27, no. 1, pp. 465–474, 2012.
- [31] K. Clark, N. W. Miller, and J. J. Sanchez-Gasca, "Modeling of GE wind turbine-generators for grid studies, version 4.5," General Electric International, Inc., Tech. Rep., 2010.
- [32] J. Slootweg, S. De Haan, H. Polinder, and W. Kling, "General model for representing variable speed wind turbines in power system dynamics simulations," *IEEE Trans. Power Syst.*, vol. 18, no. 1, pp. 144–151, 2003.
- [33] *DSATools User-Defined Model (UDM) User Manual*, Powertech Labs Inc., Surrey, BC, Canada, 2012.
- [34] *PSS/E 33.5 Model Library*, Siemens Industry, Inc., Schenectady, NY, USA, 2013.
- [35] M. E. Raoufat, K. Tomsovic, and S. M. Djouadi, "Dynamic control allocation for damping of inter-area oscillations," *IEEE Trans. Power Syst.*, 2017.
- [36] *Transient Security Assessment Tool (TSAT) User Manual*, Powertech Labs Inc., Surrey, BC, Canada, 2012.